Piezotronic Effect in Polarity-Controlled GaN Nanowires

Zhenfu Zhao,[†] Xiong Pu,[†] Changbao Han,[†] Chunhua Du,[†] Linxuan Li,[†] Chunyan Jiang,[†] Weiguo Hu,*[,†] and Zhong Lin Wang*[,†,‡]

[†]Beijing Institute of Nanoenergy and Nanosystems, Chinese Academy of Science, Beijing 100083, China and [‡]School of Materials Science and Engineering, Georgia Institute of Technology, Atlanta, Georgia 30332-0245, United States

ABSTRACT Using high-quality and polarity-controlled GaN nanowires (NWs), we studied the piezotronic effect in crystal orientation defined wurtzite structures. By applying a normal compressive force on *c*-plane GaN NWs with an atomic force microscopy tip, the Schottky barrier between the Pt tip and GaN can be effectively tuned by the piezotronic effect. In contrast, the normal compressive force cannot change the electron transport characteristics in *m*-plane GaN NWs whose piezoelectric polarization axis is turned in the transverse direction. This observation provided solid evidence for clarifying the difference between the piezotronic effect and the piezoresistive effect. We further demonstrated a high sensitivity of the *m*-plane GaN piezotronic transistor to collect the transverse force. The integration of *c*-plane GaN and *m*-plane GaN indicates an overall response to an external force in any direction.

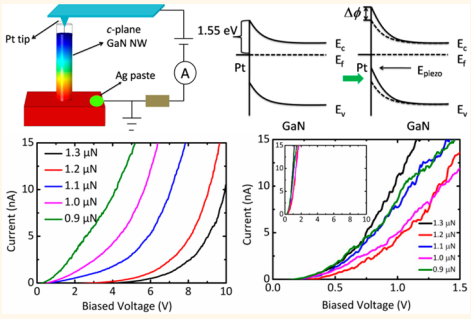

KEYWORDS: GaN · polarity · piezotronic effect

Gallium nitride (GaN), due to its direct band gap, excellent optoelectronic properties, and high physical/chemical stability,[1] has wide applications in electronic or optoelectronic devices such as light-emitting diodes,[2] field-effect transistors,[3] lasers,[4] and sensors.[5] In analogy to ZnO, GaN has a great piezoelectric property resulting from its non-centrosymmetric wurtzite structure.[6] In 2007, Prof. Z. L. Wang pointed out that, by combining the semiconductor property and the piezoelectric property, the strain applied along the piezoelectric polarization direction (*c*-axis) can generate piezopolarization charges at the two ends to modify the local Schottky-barrier height (SBH) and finally modulate the carrier transport, which is referred to as the piezotronic effect.[7−10] This novel effect builds a bridge in directly controlling electronics by mechanical stimuli and opens up various promising applications such as logical units,[11] memories,[12] nanogenerators,[13−16] piezotronic diodes,[17] piezotronic transistors,[18] and self-powered nanosensors.[19,20]

ZnO nanowires (NWs) have been the most widely used material for piezotronic devices.[21−23] A ZnO NW is synthesized by traditional bottom-up processes, such as the hydrothermal method[24] and chemical vapor deposition.[25] But these methods are not effective for growing GaN nanowires. In this study, we adopted hydride vapor phase epitaxy (HVPE) and top-down etching process to achieve polarity control on GaN piezotronic transistors, such as polar (*c*-plane) and nonpolar (*m*-plane), which can respond to any kind of motion such as normal force, sliding, and twisting. Furthermore, this study is also helpful to clarify the intrinsic differences between the piezotronic effect and piezoresistive effect, where the former is the basics of piezotronics.

RESULTS AND DISCUSSION

The polar (*c*-plane) and nonpolar (*m*-plane) GaN NWs were prepared with HVPE and top-down etching. The GaN film grown by HVPE has ultrahigh crystal qualities with a dislocation density less than 5×10^6 cm^{-2}. Figure 1a and b show SEM images of *c*-plane and *m*-plane GaN NWs at a tilt angle of 20°, respectively. It should be noted that GaN NWs are quite homogeneous in their shape, size, and alignment. The diameter and length of GaN NWs were ∼200 nm and ∼1000 nm, respectively. The crystalline quality was evaluated by XRD measurements. Figure 1c displays the XRD pattern of *c*-plane GaN. There is one peak at 34.73° observed,

* Address correspondence to (W. Hu) huweiguo@binn.cas.cn, (Z. L. Wang) zlwang@gatech.edu.

Received for review June 19, 2015 and accepted August 9, 2015.

Published online August 09, 2015
10.1021/acsnano.5b03737

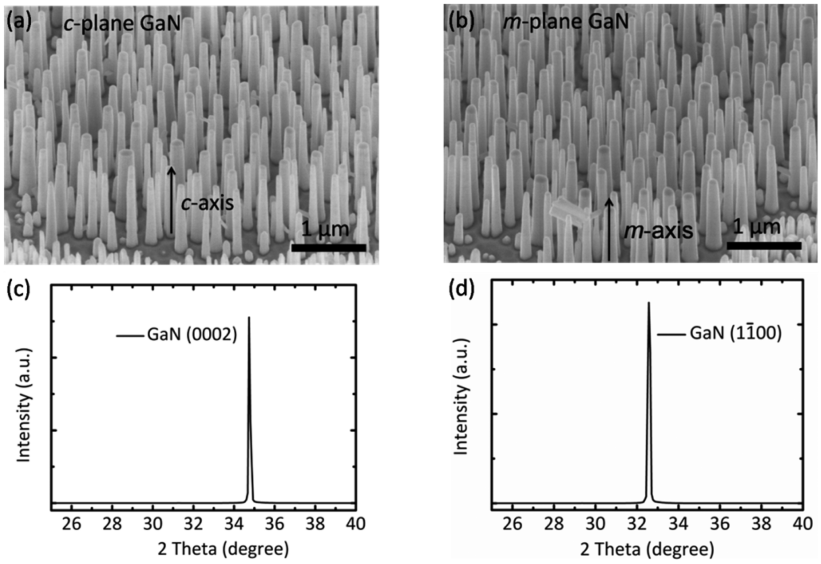

Figure 1. SEM images of (a) *c*-plane GaN NWs and (b) *m*-plane GaN NWs at a tilt angle of 20°. XRD patterns of (c) *c*-plane GaN and (d) *m*-plane GaN NWs.

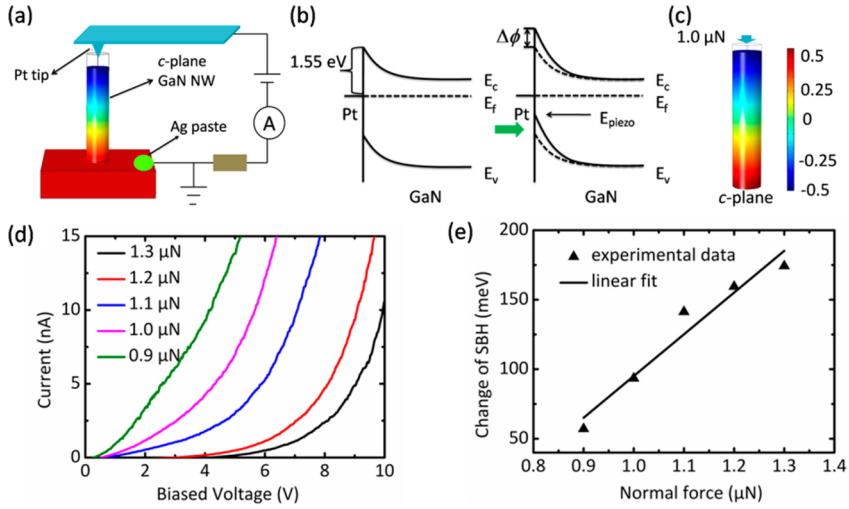

Figure 2. (a) Schematic diagram of the conductive AFM system used for nanoscale positioning and electrical measurement. (b) Schematic diagrams of the energy band illustrating the Schottky barrier formed at the metal−semiconductor interface with unstrained (left) and compressively strained ($\Delta\phi$ means the change of the SBH) (right), respectively. (c) Calculated piezopotential distribution in a *c*-plane GaN NW with length = 1000 nm and diameter = 200 nm under 1.0 μN normal compressive force by using COMSOL. (d) Typical *I*−*V* characteristics of a *c*-plane GaN NW under various normal compressive forces ranging from 0.9 to 1.3 μN. (e) Change of SBH as a function of normal compressive force. The black line corresponds to a linear fitting.

which is indexed as (0002) faces of the wurtzite-type GaN crystal.[26] The XRD pattern of *m*-plane GaN is shown in Figure 1d. The sharp peak at 32.57° stems from the *m*-plane GaN (1$\bar{1}$00) reflection. No signal is observed in the location of the GaN (0002) reflection, demonstrating that the fraction of *c*-plane GaN can be neglected.[27] This stable process has great potential in massive industry production.

I−*V* characteristics of the *c*-plane GaN NWs was measured with conductive atomic force microscopy (AFM). Figure 2a gives a schematic diagram of the measurement setup. A Pt-coated AFM probe was used to perform nanoscale contact on the top of an individual GaN NW. Silver paste was immobilized on the bottom of the GaN substrate as one electrode. Between the silver and the probe, the bias voltage was applied. The current through the NW was measured by the conductive AFM system. During the electrical measurements, various normal compressive forces were applied on the NWs by adjusting the deflection voltage of the cantilever that is linearly proportional to the magnitude of the contact force between the AFM tip and the NW.

The Schottky barrier is crucial for piezoelectric devices, which not only serves as a rectifier to determine the flowing direction of the carriers but also affects the

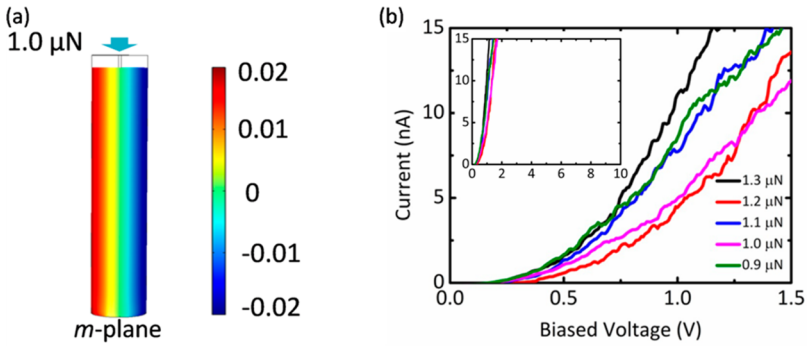

Figure 3. (a) Calculated piezopotential distribution in an *m*-plane GaN NW with length =1000 nm and diameter = 200 nm under a 1.0 μN normal compressive force by using COMSOL. (b) Typical *I*−*V* characteristics of an *m*-plane GaN NW under various normal compressive forces ranging from 0.9 to 1.3 μN. The inset is shown at the same coordinate scale as Figure 2d.

efficiency and performance of the piezoelectric nanogenerator.[28] The work function of Pt is higher than the GaN electron affinities. A Schottky junction with a 1.55 eV barrier height appears at the interface between Pt and GaN, as shown in Figure 2b. Since GaN has a noncentrosymmetric wurtzite crystal structure, a piezopotential field would be generated in the NW once a normal compressive force is applied to the piezoelectric GaN NW along the *c*-axis, controlling the electron transport by modifying the SBH.

Figure 2c shows the piezoelectric potential in a *c*-plane GaN NW simulated by COMSOL. A piezoelectric potential of ±0.48 V was generated at two ends of the *c*-plane GaN NW (200 nm diameter and 1000 nm height) under a normal compressive force of 1.0 μN along the *c*-axis.

A typical rectifying characteristic of a *c*-plane GaN NW is presented in Figure 2d, which is attributed to the Schottky junction formed with GaN and Pt. Various normal compressive forces are applied with the AFM tip to generate the piezopotential field and increase the SBH. Therefore, the current decreases by increasing the normal compressive forces from 0.9 μN to 1.3 μN. This means that the "gate voltage" can be induced with the piezotronic effect, which is called the piezotronic transistor.[29,30] The SBH is deduced according to the *I*−*V* characteristics. For simplicity, we assume an ideal Schottky diode by neglecting the shunt and series resistance and use the thermionic current−voltage relationship described by eq 1:[31]

$$I_f = AA^{**}T^2 \exp\left(-\frac{\phi_B}{k_B T}\right) \exp\left(\frac{qV_f}{nk_B T} - 1\right) \quad (1)$$

here A is the area of the Schottky barrier, A^{**} is the effective Richardson constant, T is the temperature, ϕ_B is the SBH, q is the electron charge, k_B is the Boltzmann constant, n is the ideality factor, and V_f is the voltage drop on the forward-biased Schottky diode. Equation 1 could be applied to derive the SBH change from the *I*−*V* characteristics. We can deduce the change of the SBH by[32]

$$\ln(I_f(\varepsilon_1)/I_f(\varepsilon_2)) \approx -\Delta\phi_B/k_B T \quad (2)$$

As shown in Figure 2e, the increment of SBH has a positive linearity effect on the compressive force. A 1.3 μN normal compressive force can result in an increase of 176 meV of the SBH.

The *m*-plane GaN NWs were also fabricated. Figure 3a shows the piezoelectric potential in a single *m*-plane GaN NW simulated by using COMSOL. When the normal compressive force was applied along the growth direction (*m*-axis), normal to the piezoelectric polarization axis, the two ends of the GaN NW do not exhibit any piezoelectric potential. The *I*−*V* curves of the *m*-plane GaN show rectifying characteristics but no linear dependence of SBH change on the compressive stress, as shown in Figure 3b and the inset. The variation of the *I*−*V* curve is negligible when the stress is increased, confirming that the SBH is not changed due to the absence of a piezoelectric potential along the nonpolar axis. This simulation and the experiments are quite different from the case of *c*-plane GaN (Figure 2c and d). The piezoresistive effect is a change in resistance of a semiconductor due to the change in band gap and local carrier density and has been widely observed in various semiconductor devices.[33−35] This effect changes the carrier transportation and also confuses our understanding of the piezoelectric effect. Some researchers took the asymmetry of current modulation at the forward and reverse bias to deduce the piezoelectric effect.[7,30,36,37] Our comparative study (between Figures 2d and 3b) demonstrated that the change of current transport characteristics under normal compressive force depends only on the piezoelectric polarization axis, whereas the piezoresistive effect has no polarity dependence and, thus, is totally different from the piezotronic effect observed in our experiments. This is direct evidence of the dominant role played by the piezotronic effect on the SBH.

Normal force and transverse force are two kinds of common modes. To collect the transverse force, we fixed the sample to a vertical sample stage and applied a transverse force along the *c*-axis, as shown in the scheme of Figure 4a. Figure 4b exhibits a clear sectional image scanned by AFM measurement on this vertical

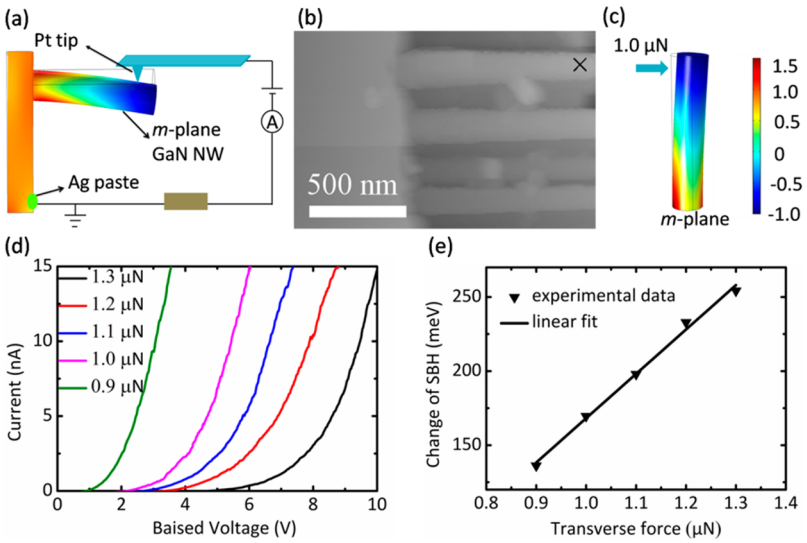

Figure 4. (a) Schematic of the AFM experimental setup. (b) AFM image of 90° tilted GaN NWs. The mark on one of the NWs indicates the location of the AFM tip during the electrical measurement. (c) Calculated piezopotential distribution in an *m*-plane GaN NW with length = 1000 nm and diameter = 200 nm under 1.0 μN transverse force by using COMSOL. (d) Typical *I*−*V* characteristics of an *m*-plane GaN NW under various transverse forces ranging from 0.9 to 1.3 μN. (e) Change of SBH as a function of transverse force. The black line corresponds to a linear fit.

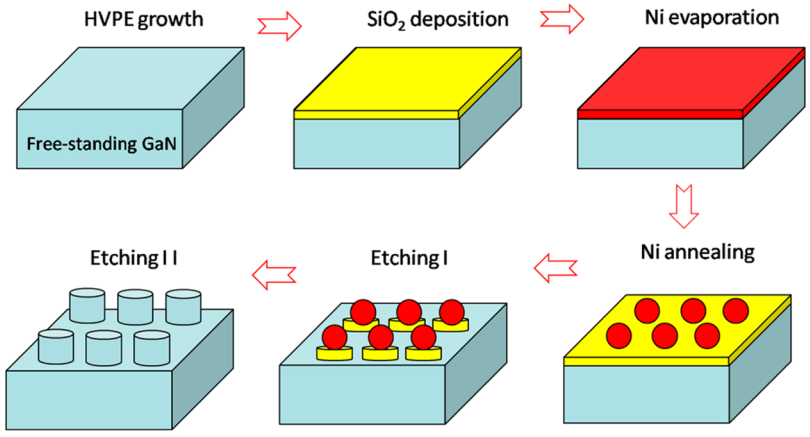

Figure 5. Schematic process flow of fabricating *c*-plane GaN and *m*-plane GaN nanowire arrays using dry-etching.

sample stage. Stable external forces were applied by pining AFM tips at the upper end of the *m*-plane GaN NW. In Figure 4c, the theoretical simulation reveals that a transverse force of 1.0 μN generates a −0.96 V piezoelectric potential at the upper end, which is larger than that (−0.48 V) of a *c*-plane GaN NW under the same normal compressive force (Figure 2c). Therefore, it will be more sensitive to modulate the electron transport by controlling the transverse force. The conductivity AFM measurements (Figure 4d) reveal that the source−drain current is rapidly pinched off on increasing the transverse force from 0.9 μN to 1.3 μN, which is consistent with the simulation. The increment of SBH of the *m*-plane GaN NW also increased linearly to 254 meV when increasing the transverse force to 1.3 μN (Figure 4e). With the integration of *c*-plane GaN piezotronic transistors and *m*-plane GaN piezotronic transistors, the piezoelectric circuit will effectively interface with any external force.

CONCLUSION

In summary, uniform and high-density *c*-plane and *m*-plane GaN nanowires arrays have been successfully fabricated using Ni nanospheres as the mask on free-standing GaN substrates. This stable and feasible process has great potential in the massive industry production of GaN nanowires. The Pt-coated AFM probe is positioned at the surface of the GaN NWs, and silver paste was adhered to the bottom GaN substrate, which forms source and drain electrodes. Theoretical and experimental results reveal that the normal compressive force effectively modulates the SBH of Pt and *c*-plane GaN, which approximately keep a linear relationship within a 1.3 μN normal compressive force. This means that external strain can act as the strain-gate to modulate the source−drain current. However, normal compressive force cannot change the electron transport characteristics in *m*-plane GaN NWs whose

piezoelectric polarization axes are turned in a horizontal direction. This is solid evidence of the piezotronic effect on the Schottky barrier and well clarifies the difference between the piezotronic effect and the piezoresistive effect. Further, an *m*-plane GaN piezotronic transistor exhibits a high sensitivity to the transverse force. The piezoelectric circuit integrated by *c*-plane GaN and *m*-plane GaN piezotronic transistors will effectively respond to any external force, which has potential applications in energy collection, biomedical sciences, strain sensors, or human−machine interfaces.

EXPERIMENTAL METHODS

Preparation of *c*-Plane and *m*-Plane GaN Nanowire Arrays. The whole fabrication process is illustrated in Figure 5. The 300 μm free-standing polar (*c*-plane) and nonpolar (*m*-plane) GaN single crystals offered by Suzhou Nanowin Science and Technology Co., Ltd. were prepared by the HVPE. Before etching, the samples were cleaned with a standard cleaning process of GaN in a bath sonicator. The 400 nm SiO_2 film was deposited on the GaN substrate by plasma-enhanced chemical vapor deposition, and then a thin Ni metal film was deposited on top of SiO_2 by electron-beam evaporation. Subsequently, the Ni/SiO_2-coated GaN substrate was annealed to form Ni nanospheres on the surface. Reactive ion etching (RIE) was used to etch the SiO_2, and the Ni mask was removed by diluted hydrochloric acid. Then, the residue of SiO_2 served as the mask for the preparation of *c*-plane and *m*-plane GaN nanowires, and inductively coupled plasma reactive ion etching (ICP-RIE) was conducted with mixture plasmas of BCl_3/Cl_2/Ar. Finally, the SiO_2 mask was removed with hydrofluoric acid wet-etching.

Electric Measurements with Conductive Atomic Force Microscope. The characterization of the piezotronic effect was carried out by an MFP-3D AFM system (Asylum Research, Inc.) with a conducting Pt-coated AFM probe. The probe has a spring constant of 2.41 nN/nm and inverse optical lever sensitivity of 98.18 nm/V. The AFM tip was positioned on top of the GaN NWs, and the current values were recorded with an applied bias. The magnitude of the force was varied by changing the deflection set point.

Theoretical Calculations. The piezoelectric potential is simulated by using a commercial software package (COMSOL Multiphysical 4.3b). Some material parameters are given as the following: transverse isotropy possesses five independent elastic constants, denoted by C_{11} = 390 GP, C_{12} = 145 GP, C_{13} = 106 GP, C_{33} = 398 GP, and C_{44} = 105 GP. The piezoelectric constants are e_{15} = −0.49 C/m^2, e_{31} = −0.49 C/m^2, and e_{33} = 0.73 C/m^2; the relative dielectric constants are k_{11} = k_{12} = 9.28, k_{33} = 10.01; and the density = 6150 kg/m^3.[13,38,39] The length and diameter of *c*-plane and *m*-plane GaN NWs used were 1 μm and 200 nm, respectively.

Conflict of Interest: The authors declare no competing financial interest.

Acknowledgment. The authors acknowledge support from the "Thousands Talents" Program for pioneer researcher and his innovation team, China, National Natural Science Foundation of China (Grant No. 51432005), and Beijing City Committee of Science and Technology (Grant Nos. Z131100006013004 and Z131100006013005).

REFERENCES AND NOTES

1. Pearton, S. J.; Zolper, J. C.; Shul, R. J.; Ren, F. GaN: Processing, Defects, and Devices. *J. Appl. Phys.* **1999**, *86*, 1–78.
2. Kim, H. M.; Kang, T. W.; Chung, K. S. Nanoscale Ultraviolet-Light-Emitting Diodes Using Wide-Bandgap Gallium Nitride Nanorods. *Adv. Mater.* **2003**, *15*, 567–569.
3. Motayed, A.; Vaudin, M.; Davydov, A. V.; Melngailis, J.; He, M. Q.; Mohammad, S. N. Diameter Dependent Transport Properties of Gallium Nitride Nanowire Field Effect Transistors. *Appl. Phys. Lett.* **2007**, *90*, 043104.
4. Johnson, J. C.; Choi, H. J.; Knutsen, K. P.; Schaller, R. D.; Yang, P. D.; Saykally, R. J. Single Gallium Nitride Nanowire Lasers. *Nat. Mater.* **2002**, *1*, 106–110.
5. Chen, C. P.; Ganguly, A.; Lu, C. Y.; Chen, T. Y.; Kuo, C. C.; Chen, R. S.; Tu, W. H.; Fischer, W. B.; Chen, K. H.; Chen, L. C. Ultrasensitive *in Situ* Label-Free DNA Detection Using a GaN Nanowire-Based Extended-Gate Field-Effect-Transistor Sensor. *Anal. Chem.* **2011**, *83*, 1938–1943.
6. Yu, R. M.; Dong, L.; Pan, C. F.; Niu, S. M.; Liu, H. F.; Liu, W.; Chua, S.; Chi, D. Z.; Wang, Z. L. Piezotronic Effect on the Transport Properties of GaN Nanobelts for Active Flexible Electronics. *Adv. Mater.* **2012**, *24*, 3532–3537.
7. Wang, Z. L. Piezopotential Gated Nanowire Devices: Piezotronics and Piezo-Phototronics. *Nano Today* **2010**, *5*, 540–552.
8. Wang, Z. L. Nanopiezotronics. *Adv. Mater.* **2007**, *19*, 889–892.
9. Wang, Z. L. The New Field of Nanopiezotronics. *Mater. Today* **2007**, *10*, 20–28.
10. Liu, Y.; Zhang, Y.; Yang, Q.; Niu, S.; Wang, Z. L. Fundamental Theories of Piezotronics and Piezo-Phototronics. *Nano Energy* **2015**, *14*, 257–275.
11. Wu, W. Z.; Wei, Y. G.; Wang, Z. L. Strain-Gated Piezotronic Logic Nanodevices. *Adv. Mater.* **2010**, *22*, 4711–4715.
12. Wu, W. Z.; Wang, Z. L. Piezotronic Nanowire-Based Resistive Switches as Programmable Electromechanical Memories. *Nano Lett.* **2011**, *11*, 2779–2785.
13. Huang, C. T.; Song, J. H.; Lee, W. F.; Ding, Y.; Gao, Z. Y.; Hao, Y.; Chen, L. J.; Wang, Z. L. GaN Nanowire Arrays for High-Output Nanogenerators. *J. Am. Chem. Soc.* **2010**, *132*, 4766–4771.
14. Wang, Z. L.; Song, J. H. Piezoelectric Nanogenerators Based on Zinc Oxide Nanowire Arrays. *Science* **2006**, *312*, 242–246.
15. Wang, X. Piezoelectric Nanogenerators-Harvesting Ambient Mechanical Energy at the Nanometer Scale. *Nano Energy* **2012**, *1*, 13–24.
16. Kumar, B.; Kim, S.-W. Energy Harvesting Based on Semiconducting Piezoelectric ZnO Nanostructures. *Nano Energy* **2012**, *1*, 342–355.
17. Yang, Q.; Wang, W. H.; Xu, S.; Wang, Z. L. Enhancing Light Emission of ZnO Microwire-Based Diodes by Piezo-Phototronic Effect. *Nano Lett.* **2011**, *11*, 4012–4017.
18. Wu, W. Z.; Wen, X. N.; Wang, Z. L. Taxel-Addressable Matrix of Vertical-Nanowire Piezotronic Transistors for Active and Adaptive Tactile Imaging. *Science* **2013**, *340*, 952–957.
19. Wang, Z. L. Towards Self-Powered Nanosystems: From Nanogenerators to Nanopiezotronics. *Adv. Funct. Mater.* **2008**, *18*, 3553–3567.
20. Hu, Y.; Wang, Z. L. Recent Progress in Piezoelectric Nanogenerators as a Sustainable Power Source in Self-Powered Systems and Active Sensors. *Nano Energy* **2015**, *3*, 3–14.
21. Yu, R. M.; Pan, C. F.; Wang, Z. L. High Performance of ZnO Nnanowire Protein Sensors Enhanced by the Piezotronic Effect. *Energy Environ. Sci.* **2013**, *6*, 494–499.
22. Lu, M. P.; Lu, M. Y.; Chen, L. J. p-Type ZnO Nanowires: From Synthesis to Nanoenergy. *Nano Energy* **2012**, *1*, 247–258.
23. Chang, Y. T.; Chen, J. Y.; Yang, T. P.; Huang, C. W.; Chiu, C. H.; Yeh, P. H.; Wu, W. W. Excellent Piezoelectric and Electrical Properties of Lithium-Doped ZnO Nanowires for Nanogenerator Applications. *Nano Energy* **2014**, *8*, 291–296.
24. Greene, L. E.; Law, M.; Goldberger, J.; Kim, F.; Johnson, J. C.; Zhang, Y. F.; Saykally, R. J.; Yang, P. D. Low-Temperature Wafer-Scale Production of ZnO Nanowire Arrays. *Angew. Chem., Int. Ed.* **2003**, *42*, 3031–3034.

25. Chang, P. C.; Fan, Z. Y.; Wang, D. W.; Tseng, W. Y.; Chiou, W. A.; Hong, J.; Lu, J. G. ZnO Nanowires Synthesized by Vapor Trapping CVD Method. *Chem. Mater.* **2004**, *16*, 5133–5137.
26. Lee, Y. J.; Kim, S. T. Growth and Properties of Free-Standing GaN Substrates. *J. Korean. Phys. Soc.* **1998**, *33*, S330–S332.
27. Waltereit, P.; Brandt, O.; Ramsteiner, M.; Uecker, R.; Reiche, P.; Ploog, K. Growth of *M*-Plane GaN (1100) on γ-$LiAlO_2$ (100). *J. Cryst. Growth* **2000**, *218*, 143–147.
28. Comjani, F. F.; Willer, U.; Kontermann, S.; Schade, W. Influence of the Metal-Semiconductor Contact by Energy Harvesting from Vertically Aligned Zinc Oxide Nanowires. *Appl. Phys. Lett.* **2014**, *104*, 143113.
29. Wang, Z. L. Progress in Piezotronics and Piezo-Phototronics. *Adv. Mater.* **2012**, *24*, 4632–4646.
30. Han, W. H.; Zhou, Y. S.; Zhang, Y.; Chen, C. Y.; Lin, L.; Wang, X.; Wang, S. H.; Wang, Z. L. Strain-Gated Piezotronic Transistors Based on Vertical Zinc Oxide Nanowires. *ACS Nano* **2012**, *6*, 3760–3766.
31. Schroder, D. K. *Semiconductor Material and Device Characterization*, 3rd ed.; Wiley: New York, 2006.
32. Zhou, Y. S.; Wang, K.; Han, W. H.; Rai, S. C.; Zhang, Y.; Ding, Y.; Pan, C. F.; Zhang, F.; Zhou, W. L.; Wang, Z. L. Vertically Aligned CdSe Nanowire Arrays for Energy Harvesting and Piezotronic Devices. *ACS Nano* **2012**, *6*, 6478–6482.
33. Kang, T. K. Evidence for Giant Piezoresistance Effect in n-Type Silicon Nanowire Field-Effect Transistors. *Appl. Phys. Lett.* **2012**, *100*, 163501.
34. He, R. R.; Yang, P. D. Giant Piezoresistance Effect in Silicon Nanowires. *Nat. Nanotechnol.* **2006**, *1*, 42–46.
35. Smith, C. S. Piezoresistance Effect in Germanium and Silicon. *Phys. Rev.* **1954**, *94*, 42–49.
36. Zhang, Y.; Liu, Y.; Wang, Z. L. Fundamental Theory of Piezotronics. *Adv. Mater.* **2011**, *23*, 3004–3013.
37. Zhou, J.; Fei, P.; Gu, Y. D.; Mai, W. J.; Gao, Y. F.; Yang, R.; Bao, G.; Wang, Z. L. Piezoelectric-Potential-Controlled Polarity-Reversible Schottky Diodes and Switches of ZnO Wires. *Nano Lett.* **2008**, *8*, 3973–3977.
38. Chen, C. Y.; Zhu, G.; Hu, Y. F.; Yu, J. W.; Song, J. H.; Cheng, K. Y.; Peng, L. H.; Chou, L. J.; Wang, Z. L. Gallium Nitride Nanowire Based Nanogenerators and Light-Emitting Diodes. *ACS Nano* **2012**, *6*, 5687–5692.
39. Fonoberov, V. A.; Balandin, A. A. Excitonic Properties of Strained Wurtzite and Zinc-Blende $GaN/Al_xGa_{1-x}N$ Quantum Dots. *J. Appl. Phys.* **2003**, *94*, 7178–7186.